PROCEEDINGS OF SCIENCE

Rapporteur on Solar and Heliospheric Physics

Cristina Consolandi[a,*]

[a] *University of Hawaii at Manoa, 2505 Correa Road, 96822 Honolulu-HI, US*

E-mail: cconsola@hawaii.edu

This rapporteur paper synthesizes the contributions presented at the 39th International Cosmic Ray Conference (ICRC 2025) concerning the structure of the Heliosphere, the mechanisms of Galactic Cosmic Ray (GCR) solar modulation, and the dynamics of Solar Energetic Particle (SEP) acceleration and transport associated with transient solar events. Several space-born experiments confirm charge-sign dependent drift effects across different solar polarities (A) and highlight particle-specific modulation differences. Sophisticated modeling approaches, including data-driven models and GPU-optimized codes, demonstrate improved capabilities in forecasting GCR transport and space radiation environments. We will give details on ground-based monitoring of short-term variations, such as Forbush Decreases (FDs) and Co-rotating Interaction Regions (CIRs), through Neutron Monitors (NMs) and Muon Detectors, establishing real-time space weather techniques. We will see new SEP results measured from space, and show promising Solar Neutron (SN) signatures that, eventually, will provide deep insights into particle acceleration sites. Finally, a list including some upcoming missions, that underscore the continuous effort to understand the highest-energy phenomena and mitigate space weather hazards, will be given.

39th International Cosmic Ray Conference (ICRC2025)
15–24 July 2025
Geneva, Switzerland

ICRC 2025
The Astroparticle Physics Conference
Geneva July 15-24, 2025

*Speaker

PoS(ICRC2025)1420

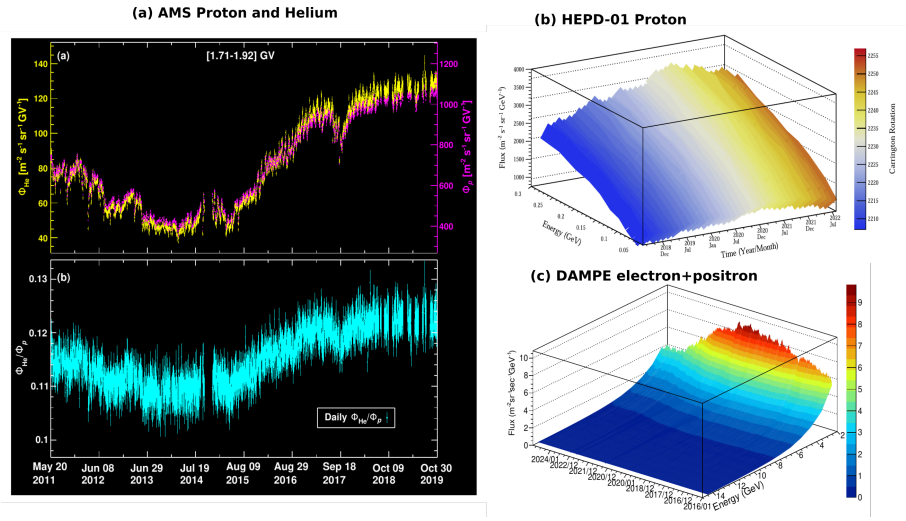

Figure 1: Long-term solar modulation effect measured by different experiments (a) AMS proton (top-violet), helium (top-yellow) and He/p flux ratio (bottom cyan) in one rigidity bin [5], HPED-01 proton flux [14] and DAMPE electron plus positron fluxes [40].

1. Galactic Cosmic Ray (GCR) Modulation and the Heliosphere

The Heliosphere is the region surrounding the Sun throughout which the influence of the solar wind plasma, with embedded magnetic field, is extended. Galactic Cosmic Rays (GCRs) propagating into the heliosphere are modulated by the solar magnetic field and the out-flowing solar wind plasma. GCR fluxes, especially at low rigidity, are significantly reduced compared to the local interstellar spectra (LIS) outside the Heliosphere. The well known anticorrelation between GCR flux and solar activity was presented by several authors in this conference. Figure 1 shows AMS proton, helium and p/He flux ratio, HPED-01 proton and DAMPE electron plus positron fluxes. As seen the GCR fluxes reach the minimum value around 2014, during solar maximum, then increase reaching the maximum around 2020 during solar minimum of solar cycle-24. This 11-year cycle of flux variation is intrinsically linked to the solar dynamo, which causes the Sun's magnetic field polarity (A) to invert at every solar maximum. The well known Parker transport equation (PTE) describes the time evolution in the heliosphere of the GCR distribution [18]

$$\frac{\partial f}{\partial t} = -\vec{V}_{sw} \cdot \vec{\nabla} f + \vec{\nabla} \cdot (K \cdot \vec{\nabla} f) + \frac{1}{3} \vec{\nabla} \cdot \vec{V}_{sw} \frac{\partial f}{\partial \ln R} \tag{1}$$

which varies under the influence of the solar wind ($\vec{V}_{sw}$) plasma convection, the diffusion and the drifts which are described by the diffusion tensor K which in turn depends on particle velocity β or equivalently to the mass to charge ration (A/Z), and due to the adiabatic energy losses (or gains) which depend on the LIS shape, *i.e.* the GCR spectral index.

Precision measurements from AMS have provided detailed insights into the relative modulation of different particle species [5, 7, 8]. At the same rigidity, Figure 1-(a) show that the effect of solar modulation is observed to be higher on the helium flux than on the proton flux. Furthermore, the hysteresis loop that has been observed between the ratio of the helium-to-proton flux and the total

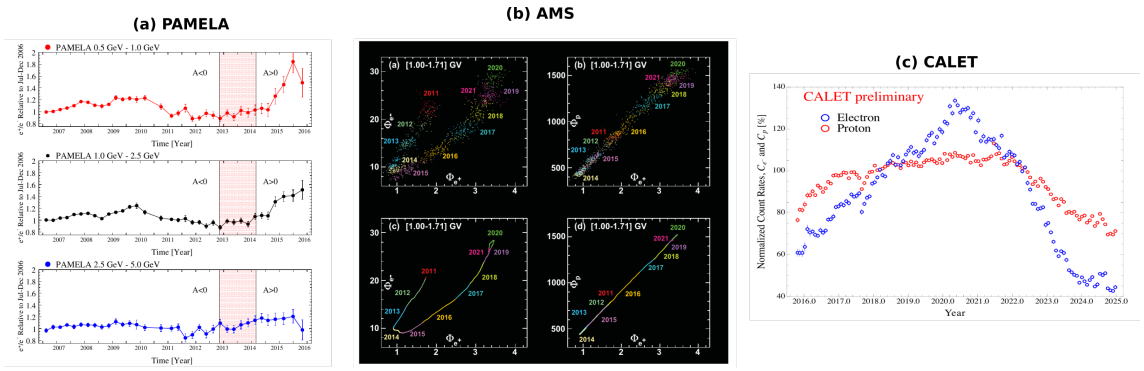

Figure 2: Charge sign solar modulation effect measured by different experiments (a) PAMELA $e^+/e-$ flux ratio in different rigidity bins [2], (b) AMS e^+, e^-, p fluxes and relative variation [6] and (c) CALET e^-, p flux comparison [49].

helium flux suggests particle-specific responses to heliospheric conditions which in this case are most probably related to the different velocity propagation in the heliosphere of the two species, i.e. different A/Z, rather than the different shape of the LIS as many authors [12, 17, 22] have pointed out. The difference in solar modulation observed in distinct nuclei with same A/Z from Lithium to Oxygen, instead, underlines the influence of the different LIS as it was specifically reported in the recent AMS collaboration publication [7].

Observations from the High-Energy Particle Detector (HEPD-01) onboard the CSES-01 satellite, from 2018 to 2022, provide critical data bridging solar cycles 24 and 25 [14]. Authors in this conference [43] showed a comparison of the GCR proton spectra and time-profiles from HEPD-01 with earlier PAMELA proton data spanning three distinct periods. This measurement offered insight into the modulation during minimum phases of cycles with differing polarities. Specifically, HEPD-01 protons observed in July 2020 (during solar cycle 24, $A > 0$) reached a flux value that was either closer to or exceeded the PAMELA proton flux recorded in December 2009 (during solar cycle 23, $A < 0$).

The DArk Matter Particle Explore (DAMPE) satellite mission, a collaboration between Italy and China launched in December 2015, reported the evolution of the electron plus positron flux over time [40]. Data from 2016 to 2024 measured by DAMPE allow for the tracking of this flux across rigidity bins (e.g., 2–3 GeV up to 13–14 GeV) during the transition between solar cycles.

1.1 Solar Modulation Drift Effect on Opposite Charged Particles

The modulation of GCRs is highly dependent on the particle's charge. Theoretical models established in 1981 [13] predict that during $A > 0$ periods, positive particles are subject to less modulation and propagate faster than negative particles. During positive polarity epochs ($A > 0$), positive charged particles exhibit a primary drift in the heliosphere, entering from the poles and exiting through the equator. The reverse path is followed by negative charged particles. This structure is organized by the heliospheric current sheet surface, which serves to divide the regions characterized by positive and negative solar magnetic field lines. This phenomena, known as drift effect of opposite charged particles, was already reported by PAMELA [1, 2] and AMS [3, 6]. In the

present ICRC meeting, this typical charged sign effect of solar modulation between protons (positive charge) and electrons (negative charge) was reported by the DAMPE collaboration with the CALET instrument data on the International Space Station [49]. Figure 2 collects the observation of the typical charged sign effect of solar modulation between protons, electrons and positron observed by PAMELA [2], AMS [6] and CALET [49]. In particular, Figure 2-(c) show how the proton flux reaches the maximum value and remains stable longer compared to the electron flux that continue increasing until the maximum flux reached in solar minimum around 2020.

1.2 Advanced GCR Transport Modeling and Computation

To find a solution of the PTE is not easy task. In general there are two approaches that may be followed to find a solution for the solar modulation of GCRs: (1) a comprehensive 3-Dimensional solution and (2) the use of a simplified version of the PTE which gives the simple Force Field Approximation (FFA) solution which employs only one parameter, i.e. the heliospheric modulation parameter ϕ. Both approaches have advantages and disadvantages. The FFA method is easy to implement, can provide a direct insight for the basic understanding of the physical process, but is unable to capture the proper effect that give the correct understanding of the physics. The 3-Dimensional approach is able to incorporate many physical processes in details but on the downside they can reach high complexity with too many parameters and high level of degeneracy.

In this conference, a comprehensive 3-Dimensional numerical heliospheric modulation model was employed for detailed computations of the GCR behavior [50]. This model is rigorously validated against long-term, high-quality observational datasets utilizing PAMELA and AMS proton covering from 2006 to 2011 and from 2011 to 2019, respectively. On the other hand, other authors in this conference [61, 62] developed methods for calculating the FFA ϕ parameter from neutron monitor (NM) data and validated with monthly to daily AMS data. In the effort to expand the model capability to hourly cadence, they also presented both challenges and possibilities for real-time monitoring.

To enhance the efficiency of simulating GCR transport for the 3-Dimensional approach, high-performance computing techniques were shown by some authors [29]. These authors developed a Monte Carlo simulation code named COSMICA built upon Stochastic Differential Equations coupled with a parameter search interface known as SDEGNO. The integration of COSMICA with SDEGNO allows for extremely efficient scanning of the vast parameter space of the PTE, and this optimization demonstrated the ability to reduce computational time by up to three orders of magnitude compared to existing codes like HELMOD.

An alternative method to give a simple solution to the PTE, so that it can be widely used without loosing in physics accuracy, was explored in this conference [59]. A comprehensive modeling effort, that involve a data-driven approach, was shown by the use of the LxPg-model specifically designed for GCR transport in the Heliosphere. This model incorporates various physics processes and explicitly accounts for charge-sign dependence. The utility of the LxPg-model extends beyond fundamental research, serving as an application tool for space weather radiation forecasting and the calculation of the total effective dose received by astronaut.

1.3 Co-rotating Interaction Regions and GCR Periodicity

A short-scale phenomena creating recurrent variations in the GCR flux, is related to Co-rotating Interaction Regions (CIRs). Solar magnetic structures, known as Coronal Holes, are regions on the Sun where the magnetic field expands openly into the heliosphere, embedded within the solar wind flow. CIRs form far from the Sun when the fast solar wind stream overtakes and compresses the slow solar wind stream. CIRs are associated with a decrease in GCR flux exhibiting the characteristic ~27-day periodicity, corresponding to the Sun's rotation period. From space, this effect was already measured and analyzed by different authors [4, 16]. In this conference, multi-spacecraft observations confirmed this periodicity for galactic protons [53]. Data collected between 2018 and 2019 by HEPD-01 (onboard CSES-01) were analyzed alongside data from other experiments, including EPHIN, ERNE, and AMS. Wavelet analysis using a Morlet function was applied to the detrended proton fluxes. Figure 3-left shows the temporal evaluation of the relative (detrended) proton fluxes measured by HEPD-01, and the results of the wavelet analysis applied to the daily HEPD-01 proton flux, from August 2018 to August 2019. The 27-days periodicity is mostly evident in the first period. Figure 3-right shows the resulting amplitude of the 27-day periodicity (A_{27}) versus rigidity for different experiments. A_{27} was observed to vary non-monotonically as a function of rigidity with specific local minimum observed around 0.4 GV, a feature hypothesized to be related the particles accelerated by the CIR driven shocks. Further studies, utilizing 3D numerical models with MHD background and GCR transport simulations, have investigated the detailed effects of CIRs on GCR propagation [41]. These studies confirm that the effects of CIRs are distinct across different particle species based on their mass. Specifically, the effect of CIRs on protons is found to be weaker than the effect on ^4He, but stronger than the effect on ^3He. A possible explanation may be related to their different mass to charge ratio, or equivalently a different β value, resulting in a different diffusion coefficient. This particle dependence of the recurrence amplitude with GCR rigidity, applicable to both protons and helium nuclei, also confirmed the presence of a turning point in the A_{27} variation around 0.3-0.4 GV.

2. GCR ground Measurements: Neutron Monitors and Muon detectors

Neutron Monitors (NMs) are ground detectors, active since the 1950s, that measure secondary cosmic rays produced by GCRs by means of nuclear interaction with Earth's atmosphere atoms. NM stations are distributed across the world, working together as a giant spectrometer, known as the Global NM Network (GNMN). At present, there are more than 80 active NM stations. Similarly, muon detectors provide additional information about secondary produced in the atmosphere with the Global Muon Detector Network (GMDN) constituting of 5 stations.

2.1 Leader Fraction as a Proxy for Spectral Index Variation

The leader fraction (LF) is a parameter that can be derived from NM data, and measures the prompt component of the air shower induced by GCRs. The LF is defined as the fraction of first pulses identified in multi-counter time-delay histograms to infer spectral variations of primary cosmic rays. Prior works demonstrated the potential of the LF method as an independent spectral diagnostic [21]. Being the NM mostly sensitive to the GCR in the tens of GV rigidity range, the

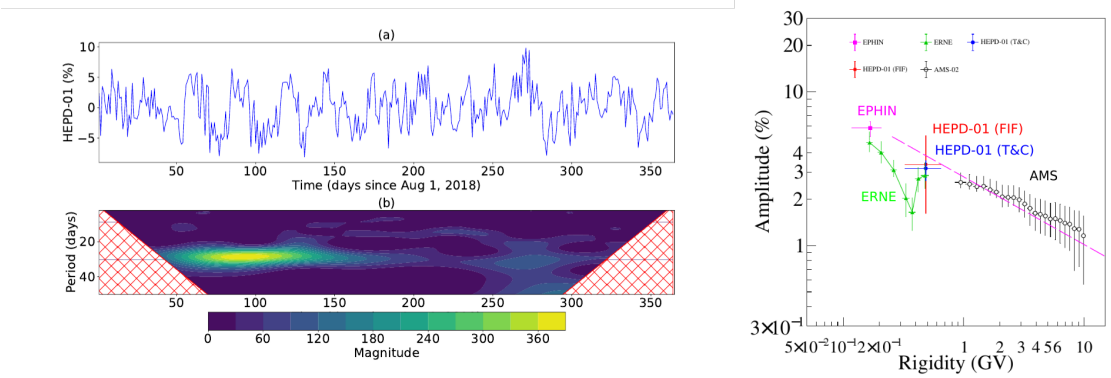

Figure 3: (Left) Top: temporal evaluation of the relative (detrended) proton fluxes measured by HEPD-01. Bottom: wavelet analysis of daily HEPD-01 proton flux for the August 2018-August 2019 period (Right) Reconstructed rigidity dependence of A_{27} for GCR proton data observed by EPHIN (magenta marker), ERNE (green markers), HEPD-01 (blue and red markers) and AMS-02 (black markers) from September 2018 to February 2019. Dashed line represents the fit with a simple power law. [53]

LF can therefore be directly related to the high-energy part of the cosmic ray spectrum. In this conference, analysis of the three-month averages of the LF plotted against the total count rate at the Princess Sirindhorn NM (PSNM) in Thailand revealed significant solar cycle dependence [23]. Specifically, a hysteresis effect was observed in solar cycle-24. The hysteresis underlines how the shape of the cosmic ray spectrum underwent a change in the period spanning before and after the solar magnetic polarity reversal that occurred between 2012 and 2014. Importantly, the hysteresis pattern observed for solar cycle-24 is noted to be distinct from the pattern observed for cycle-25.

2.2 Coronal Mass Ejection, Forbush Decrease and Leader Fraction

A Coronal Mass Ejection (CME) is a large-scale release of plasma, with accompanying magnetic field, from the Sun's Corona. When the resultant Interplanetary CME (ICME) travels through space, it generates a magnetic disturbance in the Interplanetary Magnetic Field [20]. This disturbance subsequently causes a temporary reduction in the intensity of the GCR flux, known as Forbuch decrease (FD) [11]. The analysis of FD profiles yields specific information about GCR interaction with local magnetic fields. The decreasing phase of an FD provides information regarding the interaction of GCRs with the local magnetic disturbance. Conversely, the recovery phase of the FD offers insight into the processes of diffusion and drift of GCRs within the heliosphere. An example of a detailed analysis of a FD with related anisotropy was shown in this conference for November 2021 event using GMDN and GNMN data [37]. Figure 4 shows the result of a Bayesian estimation of the anisotropy components for this event at 50 GV GCRs. The blue vertical line indicates the arrival time of the interplanetary shock, and the interval bordered by green vertical lines corresponds to the period when Earth was inside the interplanetary CME. Black points are the density based on NM and muon detector measurements which were derived by fitting power-law functions. Red points are the result of a Bayesian estimation. Colored maps below display the time-series anisotropy. The size of the FD variation is around 1%, and the anisotropy analysis, with power-law fit, show a bidirectional flow inside the CME cloud. Other authors [48] used both

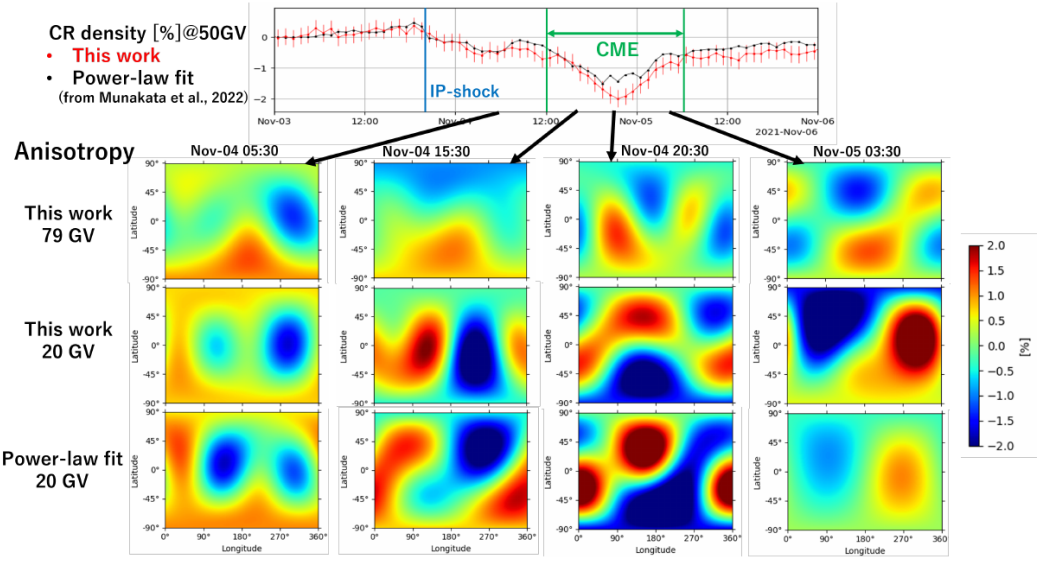

Figure 4: Result of a Bayesian estimation of the anisotropy components for November 2021 event. (Top) The blue vertical line indicates the arrival time of the interplanetary shock, and the interval bordered by green vertical lines corresponds to the period when Earth was inside the interplanetary CME. Black points are the density based on NM and muon detector measurements which were derived by fitting power-law functions. Red points are the result of a Bayesian estimation (Bottom) Result of the anisotropy study at different rigidity. [37]

GMDN and the GNMN to perform hourly FD analysis. A global fitting of GCR rigidity spectral model with anisotropy up to second order, and the LF technique was applied to understand the time variation during the FD event. The global-fit method, specifically, relies on calculating the fractional intensity change relative to a pre-event reference interval, which allows for the calculation of the change in the GCR spectral index during the FD event. The LF analysis, instead, is performed with time delay distributions between successive neutron detections by each counter of the South Pole NM. Both methods provide consistent results for spectral index variations during five major FDs between 2015 to 2023 and agreed with the daily space-based observations by AMS.

2.3 Yield Function and Latitude Survey

To independently derive the primary GCR flux from the NM count rate, the secondary showers in the atmosphere and the detector response must be known. All these information are incorporated in the Yield Function (YF) that is usually derived by extensive Monte Carlo (MC) simulations where all the physics related to the charged particles interactions with the Earth's atmosphere atoms are modeled and simulated together with the ambient detector conditions and response. In addition, NMs are deployed at different latitude on Earth and due to geomagnetic cutoff effects each station is sensitive to different rigidities of the GCR spectra. To know the detector response at different geomagnetic latitudes a latitude survey is highly desirable. During a latitude survey the same NM is moved at different latitudes, usually aboard of ships, so that it's exposed to different GCR secondary flux according to the local geomagnetic cutoff. Information on the NM YF and detector calibration

can also be derived from data taken during a latitude survey. In this conference, preliminary results from the 2023–2024 latitude survey conducted aboard the ARAON Icebreaker reveal variations in the Dorman parameters (N_0, α, κ) when comparing different tube types (T3-BP28 Leaded, T2-BP28 Unleaded, T1-LND Leaded) [51]. This variability indicates that the instruments exhibit sensitivity to both their physical construction and the environmental modulation encountered across a broad range of geomagnetic cutoff rigidities.

3. Solar and Heliospheric: Multi-messenger Proxy

Beyond the standard detectors specifically designed to study GCR solar modulation and the Sun related phenomena, during this particular ICRC edition many contributions were dedicated to data taken from instrument designed for other purposes that, anyway, demonstrated to serve as solar proxy, underling the importance of a multi-messenger and interdisciplinary approach in data analysis and research. In this section a summary of the most interesting contributions is given.

3.1 Auger Observatory as a Solar Activity Proxy

The Pierre Auger Observatory, located in Malargüe, Argentina, demonstrated that scaler data are robust proxy for monitoring solar activity [58]. The Auger scaler rates measure low-energy cosmic rays, corresponding to a deposited energy range of 15 – 100 MeV, with primary GCR energies spanning approximately from 10 to 10^3 GeV. Techniques such as Singular Spectrum Analysis and Continuous Wavelet Transform were also applied to correlate these rates with other solar indices, such as the Sunspot Number (SSN) and the Interplanetary Magnetic Field (IMF) intensity. Interestingly, a 1-year shift in correlation was observed.

Another interesting result came from AERA data [45]. Beyond its original design for extensive air showers, the AERA array at the Pierre Auger Observatory also found to have broader potential for studying solar activity and its associated effects on the Earth's atmosphere and space weather monitoring. In particular, authors reported on radio blackouts in coincidence with NOAA reports and observed a clear correlation between the Maximum Usable Frequency (MUF) and the noise level in the 30-40 MHz band in AERA data. In addition, about 200 temporal coincidence of Solar Radio Burst (SRB) were recorded in coincidence with the e-Callisto antenna network and coincidence rate up to 60% between the SRB observed by SWAVES and AERA was found.

3.2 Galactic Cosmic Ray Interaction and Solar Gamma-Ray Flux

GCRs interacting with the solar atmosphere produce secondary γ-rays. This steady-state γ-ray emission is divided into two primary components: Hadronic disk component and Inverse Compton (IC) Spatially Extended Component. The Hadronic disk component arises from hadronic cascades initiated by GCR protons and nuclei interacting within the solar atmosphere. The IC Spatially Extended Component is, instead, generated when GCR electrons interact with solar photons. A contribution in this conference reported on the flux variation of these two components based on Fermi Large Area Telescope observations [57]. It was shown that the Hadronic disk component exhibits a strong anticorrelation with the SSN, the AMS GCR proton flux, while the IC extended flux component shows no clear correlation with solar activity across all observed time intervals.

Another contribution on a 3D MC calculation of the IC emission from the Sun that was implemented within the FLUKA simulation code was reported [44]. This advanced model allows for the calculation of gamma-ray emission in complex geometries, including the presence of magnetic and electric fields, and also incorporates synchrotron radiation emission along particle trajectories.

3.3 Sun and Moon Shadow Observations

The ALPAQUITA Air Shower Array in Bolivia has successfully observed both the Moon shadow and the Sun shadow [34]. The Moon shadow was clearly detected, showing a deficit ratio of approximately 10 standard deviations. The Sun shadow was also observed, showing a smaller deficit ratio of about 5 standard deviations. The observation of a smaller deficit ratio for the Sun shadow compared to the Moon shadow suggests an interaction mechanism unique to the solar environment. This is hypothesized to be caused by the scattering of GCRs by the complex coronal magnetic fields present during the active solar phase. Additionally, a marginal significance (1.5σ) of a northward displacement was found during the "Away"-sector dominant period of the Sun Parker spiral, consistent with the Lorentz force deviation for positive charged particles.

Another contribution explored theoretical mechanisms leading to the detection of over-abundant gamma-like signals around the Solar disk [30]. This phenomenon is hypothesized to arise from smeared and bent electron-pairs spiral. The core concept posits that GCRs at high energies (TeV to PeV range) that skim close to the Sun can initiate air showers, potentially producing neutral or charged mesons. Authors suggested that the resulting signal, which may be a true γ-ray or a γ-ray-like signal associated with the spiraling of electron-pairs, could be detected on the ground by instruments such as HAWC. Such analyses should address two distinct regions that can be addressed as "Shadow-positive," and "Shadow-negative" that are actually observed around the Sun position in HAWC data [9].

4. Solar Energetic Particles, Solar Neutrons and Ground Level Enhancements

Solar Energetic Particles (SEPs) are particles accelerated by the Sun during explosive events such as solar flares and CMEs. After been accelerated, SEPs follow the complicated structure of the Interplanetary Magnetic Field (IMF), so that, when they arrive at Earth, their spatial distribution is greatly affected by propagation processes, modifying their arrival time, intensity, duration, and anisotropy. During strong solar flares, the Sun can also emit energetic neutrons, called Solar Neutrons (SNs), created in interactions of SEPs with nuclei in the Sun's atmosphere. Since SNs are not affected by the IMF, they retain direct information about the nuclear reactions happening near the SEP acceleration site. When an SEP or an SN event occurs at high energy (GeV), it may initiate a cascade of secondary particles in the Earth's atmosphere that can be detected on the ground by NMs, *i.e.* Ground Level Enhancement (GLE). In this conference, NM and muon detector complemented observations from the May 11, 2024 solar event (GLE 74) [25] suggest that the associated shock wave and ICMEs actively influence the arrival direction of the particles, resulting in a non-isotropic behavior observed in the West-East direction. The comparison of the muon-to-neutron ratio across different detector sites (ORCA in the South Pole and ICaRO in Tenerife) showed different behavior, which is attributed to rigidity dependence. The detailed analysis of GLE 74, and coincident FD, using NM data was shown by [46, 47] who derived the rigidity spectra and pitch angle distribution.

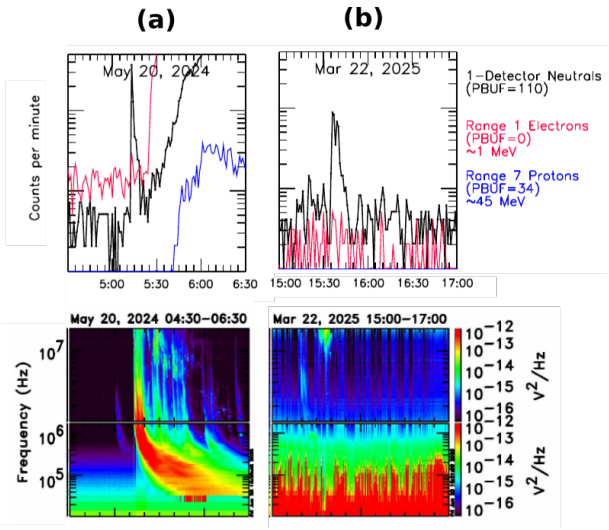

Figure 5: Figure adapted from [39]. Top: 1-minute cadence count rates from EPI-Hi/HET in 2-hour time windows during the 9 γ-ray flares, showing 1-detector neutral rates (black), 1 MeV electrons (red) and 45 MeV protons (blue). Bottom: Dynamic radio spectra from FIELDS/RFS on Parker in 2-hour time windows during the 9 γ-ray flares. (a) Typical example of charge interaction signal; (b) Neural interaction signal signature

As previously mentioned, SNs are produced during energetic solar flares. The production mechanism involves nuclear reactions where accelerated ions, predominantly protons and α-particles, interact with the dense solar atmosphere. Since SNs propagate along straight lines they may retain direct information about the acceleration site and may help to understand the acceleration mechanism [27]. If SNs possess sufficient energy, they can reach Earth and initiate an atmospheric shower cascade which is detectable on the ground as a GLE, similar to conventional GLEs induced by SEPs. Analysis of possible NS events are presented in [52]. To distinguish between the two type of GLEs the NM location is the smoking gun. GLEs observed at high geomagnetic cutoff latitudes are only initiated by SNs because SEP of ~1 GV cannot reach equatorial latitudes. Sites characterized by low-latitudes and high-altitude are considered optimal locations for SN detection. In this conference, authors reported on the status of the Haleakala NMs, HLEA and THIMON, deployed on Maui (3052 m altitude, 20°42′N, 156°15′W) at low-latitude with a vertical cutoff of 12.91 GV and an atmospheric depth of ~700 g cm^{-2} [24]. The summit of Haleakala is an ideal position for SN detection: the high-altitude minimizes SN absorption in the atmosphere, and, in addition, the low-latitude maximizes the Sun's elevation, thereby increasing exposure. All stages of the deployment we completed and HLEA and THIOMON are now taking new data.

In this conference, simulation studies using FLUKA code investigated the interaction of 0.1–10 GeV SNs with the Earth's atmosphere [35]. The simulations concluded that the Bare Counter (BC) over the NM count ratio is higher for SN events compared to the ratio derived from GCRs. This established the BC/NM ratio as a promising technique for solar neutron detection, especially at locations with high geomagnetic cutoff rigidities, such as PSNM, HLEA and THIMON.

4.1 Gamma-Ray Flares and Neutrals for Solar Neutron Detection from Space

Interestingly, observations of Solar Gamma-Ray Flares and Neutrals may be the alternative way to detect NS from space. In this conference, it was reported on the observations of solar γ-ray flares conducted by the ISIS/EPI-Hi/HET instrument on the Parker Solar Probe (PSP) that revealed specific signatures of neutral particles [39]. The detection mechanism for neutrals in HET involves an incident neutral particle passing undetected through the outer guards. It then interacts through Compton scatter to produce an electron, and subsequently leaves a measurable signal in the sensitive regions of the detector. Nine distinct events showed increases in the detector neutral counts without corresponding simultaneous jumps in the energetic proton or electron rates. Figure 5 shows an example of two events: May 20th 2024 which appears to have a typical charged particle interaction signal, and March 22nd 2025 solar event which shows to have a neutral interaction signal. Analysis of the March 22nd 2025 suggests that particles depositing 3–10 MeV in the detector may be attributed to incident SN with energies around 20–30 MeV.

4.2 Solar Energetic Particle CSES-01 Observation from Space

SEP measurements by the China Seismo-Electromagnetic Satellite (CSES-01) where reported by [33, 43, 54]. These works present an in-depth analysis of selected major solar events utilizing data acquired by the High-Energy Particle Detector HEPD-01 and the related particle detector HEPP-L onboard CSES-01. The CSES-01 has provided critical observations of the Sun-Earth environment, spanning the transition between solar cycle-24 and -25 (2018–2022) including a series of SEP events. The low-Earth orbit platform of CSES-01, indeed, allows for linking the low- to the high-energy measurements, a crucial junction point for characterizing the dynamics of SEPs during major events as reported in [10]. An example of the detector capability is summarized in Figure 6, that shows the time evolution of the October 2021 SEP event (GLE 73) [15]. CSES-01 data facilitated a good velocity-dispersion analysis. By fitting all observational points, this analysis allowed for the extraction of key event parameters, including the particle path-length (L) and the Solar Particle Release (SPR) time. Importantly, the HEPD-01 data was able to constrain the SEP spectral shape at higher energies.

4.3 Solar Energetic Particle, Acceleration and Dynamics

The acceleration of SEPs is generally attributed to two main processes: magnetic reconnection and diffusive shock acceleration (DSA). In magnetic reconnection process during a solar flare, the acceleration occurs in close proximity to the solar surface. In DSA, the acceleration occurs at the shock front driven by an ICME traveling through interplanetary space. The two mechanism may have indistinct spectra features and particle composition, but since they usually come together, it's often difficult to asses which mechanism gives the major contribution to the SEP acceleration.

A study focusing on an eruptive flux rope event utilized γ-ray light curves to dissect the acceleration mechanism [55]. Two γ-ray peaks were observed. The first γ-ray peak was interpreted as evidence for the efficient acceleration of electrons and, most likely, ions. The second γ-ray peak, however, was characterized as an Fe-rich event, where the particles were accelerated via the magnetic reconnection, or null point reconnection. Details of the analysis can be find in [19].

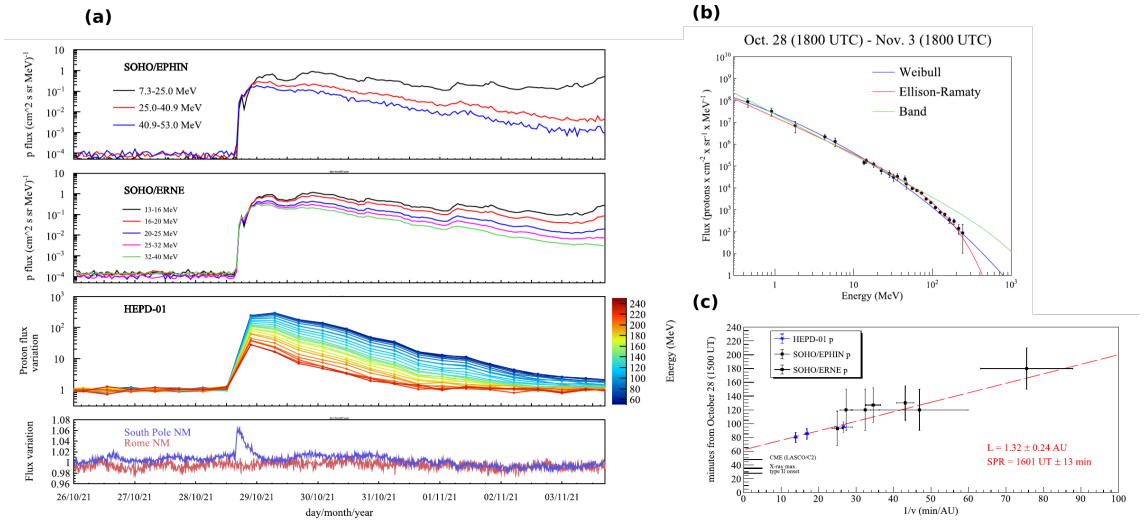

Figure 6: Figures adapted from [15]: (a) Time evolution of the 2021 October solar energetic particle event, as seen by EPHIN and ERNE (first two panels)—both located on the SOHO spacecraft placed in the Lagrangian Point L1—in 3 and 5 energy intervals, respectively. The passage of the shock is evident in both the time-profiles. A >300x variation of 50 MeV proton fluxes was registered by the High-Energy Particle Detector at Low-Earth Orbit (third panel). Finally, time-profiles of two Neutron Monitors on ground (South Pole and Rome) are shown in the fourth panel. (b) The pure, energy-extended event-integrated solar proton spectrum obtained by combining the observations of the High-Energy Particle Detector with the ones from ACE, SOHO/EPHIN, and SOHO/ERNE. The vertical error bars account for both statistical and systematic uncertainties, plus the 20% added to account for other uncertainties. The blue, red and green curves represent the fit performed by using the Weibull, Ellison-Ramaty and Band functions respectively. (c) Onset time of the October 28 solar event versus 1/velocity, using the High-Energy Particle Detector (HEPD-01), EPHIN and ERNE proton data. The red dashed line represents the fit to the experimental points, while the short horizontal lines on the y-axis indicate the onset of the type II radio emission, the maximum of the X-ray emission and the first observation of the coronal mass ejection by LASCO/C2. The path-length L and Solar Proton Release parameters (see text), extracted from the fit, are shown in the bottom-right corner of the plot. As can be seen, HEPD-01 provides proton measurements at higher energies with respect to EPHIN and ERNE.

The July 23, 2024, Fe-rich SEP event provides a crucial case study that was reported in this conference [28]. This event was linked to an X-14 class flare and a fast halo CME. Even if ACE, STEREO-A, and Parker Solar Probe (PSP) were not well mangetically connected to the solar flare, they all measured high Fe/O ratios that were relatively energy-independent. Solar Orbiter, that was well magnetically connected to the solar flare, reported a strong energy-dependent Fe/O ratio, showing low values at 1–few MeV/n. The existence of high Fe/O ratios is addressed by two competing explanations: (1) the observed particles are direct flare material captured by well-connected observers, or (2) the particles are remnant suprathermal flare material that was subsequently accelerated by perpendicular shocks. Magnetic connection analysis suggested that ACE, STEREO-A, and PSP were located at large distances (greater than 50 degrees) from the flare source. For this reason it's still not clear what flare directly contribute. The authors suggested that the evaluation of the shock parameters (e.g., nose vs. flank position) at the connection point is

necessary to better understand this event.

Analysis of certain solar energetic electron events revealed an unusual characteristic: a bump-like spectral break occurring above 20 KeV [63]. The model posits that the power-law population is likely produced by flare-related acceleration processes situated high in the solar corona. The bump population, however, is hypothesized to be due to a secondary acceleration process, potentially related to the CME acting upon the pre-existing power-law population. Interestingly, authors concluded that this process may not involve shock acceleration.

4.4 Solar Energetic Particles and Transport

For a comprehensive understanding of the SEP physics, beyond particle acceleration, the transport from the Sun to Earth is also necessary to be investigated. A contribution in this conference was dedicated to the transport of SEP and the relative importance of a turbulent drift was analyzed [38]. Full-orbit simulations investigated how turbulence affects the SEP latitudinal drift. The resulting reduction in drift is much weaker than predicted by theoretical estimates. Moreover, the reduction in drift is observed to be smaller for high-energy SEPs. This confirms that gradient and curvature drifts remain significant factors in SEP transport, particularly for high particle energies and heavy isotopes. Another contribution was addressing the Corotation Effects and the East-West asymmetry on SEPs [32]. Corotation, usually considered negligible, was shown by simulations to potentially influence SEP event profiles. These simulations suggest that corotation could introduce an East-West difference in the observed decay phases of SEP events. Observational data indeed support this, showing a difference in SEP decay phases depending on the observer's location, which is consistent with the hypothesized corotation effect.

5. Space Weather Applications and Future Outlook

Recently more and more interest has grown around space weather, now-casting and forecasting design. In this conference, many contributions were dedicated to the development of GCR models that also supports crucial space weather applications. Based on the cosmic ray transport equation, one example is a GCR numerical model specifically designed for solar modulation and developed to accurately reproduce data from both the PAMELA and AMS instruments [42]. This model is utilized to calculate the astronaut radiation dose rate in the global heliosphere by adopting unshielded isotropic fluence-to-dose conversion coefficients. This model is capable of tracking radiation doses across solar cycle minima and maxima. Other authors reported on the data-driven LxPg-model, which accounts for GCR transport and charge-sign dependence, and was specifically developed for space weather radiation forecasting and calculating the total effective dose [59].

These contributions demonstrated to have achieved progressive knowledge on the radiation doses induced by GCRs. But what about the SEPs? Historical evidence of Extreme Solar Particle Events (ESPEs) is preserved in cosmogenic isotopes (^{10}Be, ^{14}C, ^{36}Cl) [60]. ESPEs are orders of magnitude higher than any event recorded during the space era. Present research suggests that ESPEs are more likely to occur during periods of weak-to-moderate solar activity [36]. The occurrence rate is estimated to be approximately 1/1500 years. If an event like this would happen in our technological era, it would have catastrophic consequences for present society. From here the necessity to continue studying and to advance technology and instrumentation for future missions.

New missions, that were presented in this conference, will include: the CSES Program, that with the HEPD-02 detector onboard CSES-02, already launched on June 14th 2015, will provided critical data for future spanning solar cycles [33]; the Thai Space Consortium Satellites planned missions include the 1st Thai Space Consortium Satellite (TSC-1) which will carry the Polar Orbiting Ion Spectrometer Experiment (POISE) Payload [26]; the Thai-Chinese Hodoscope, that is being designed for observing cosmic ray electrons, SEPs, and Lunar Albedo Ions [56]; Lunar Energetic Particle Environment with the LunPAN project, that is dedicated to providing a comprehensive study of the Lunar Energetic Particle Environment [31].

6. Conclusion

The ICRC 2025 presentations demonstrate robust progress in solar and heliospheric physics, driven by both high-precision satellite data (e.g., AMS, DAMPE, CALET and HEPD-01) and sophisticated ground-based networks (GMDN, NMN). Crucial insights were gained into the charge-sign dependence of solar modulation, reinforcing the fundamental role of magnetic drift effects. Modeling efforts continue to become more refined, leveraging GPU acceleration (COSMICA) and data assimilation (LxPg) to provide increasingly accurate representations of GCR transport and subsequent space weather forecasting. The identification and detailed characterization of solar neutral emissions and complex SEP acceleration sites, including null point reconnection and unique electron spectral structures, highlight the dynamic nature of particle acceleration during transient events. Future missions promise to further expand our observational capabilities, particularly regarding lunar and high-latitude particle environments.

References

[1] Adriani, O. et al.Ten yeas of PAMELA in Sapce. La Rivista del Nuovo Cimento. **10**, 473 (2017).

[2] Adriani, O. et al. Time Dependence of the Electron and Positron Components of the Cosmic Radiation Measured by the PAMELA Experiment between July 2006 and December 2015. Phis. Rev. Let., **116**, 241105 (2016)

[3] Aguilar M., et al. The Alpha Magnetic Spectrometer (AMS) on the international space station: Part II — Results from the first seven years, Phys. Rep. **894**, 1 (2021).

[4] Aguilar M. et al. Periodicities in the Daily Proton Fluxes from 2011 to 2019 Measured by the Alpha Magnetic Spectrometer on the International Space Station from 1 to 100 GV Phys. Rev. Lett. **127**, 271102 (2021).

[5] Aguilar M. et al., Properties of Daily Helium Fluxes, Phys. Rev. Lett. **128**, 231102 (2022).

[6] Aguilar M. et al., Temporal Structures in Positron Spectra and Charge-Sign Effects in Galactic Cosmic Rays, Phys. Rev. Lett. **131**, 151002 (2023).

[7] Aguilar M. et al., Solar Modulation of Cosmic Nuclei over a Solar Cycle: Results from the Alpha Magnetic Spectrometer Phys. Rev. Lett. **134**, 051001 (2025).

[8] Aguilar M. et al., Antiprotons and Elementary Particles over a Solar Cycle: Results from the Alpha Magnetic Spectrometer, Phys. Rev. Lett. **134**, 051002 (2025).

[9] Albert, A. Discovery of Gamma Rays from the Quiescent Sun with HAWC. Phys. Rev. Lett., **131**, 051201 (2023).

[10] Bartocci, S. et el. Multispacecraft Observations of Protons and Helium Nuclei in Some Solar Energetic Particle Events toward the Maximum of Cycle 25. ApJ, 974, 176 (2024)

[11] Cane, H. V. Coronal Mass Ejections and Forbush Decreases. Space Science Reviews, 93, 55 (2000)

[12] Corti C. et al., Numerical modeling of galactic cosmic-ray proton and helium observed by AMS-02 during the solar maximum of solar cycle 24, Astrophys. J. **871**, 253 (2019)

[13] Jokipii, J.R. and Thomas, B. Drift Effect of Drift on the Transport of Galactic Cosmic Rays IV. Modulation by a Wavy Interplanetary Current Sheet. The Astrophysical Journal, **243**, 1115-11-22 (1981).

[14] Martucci, M. et al. Time Dependence of 50–250 MeV Galactic Cosmic-Ray Protons between Solar Cycles 24 and 25, Measured by the High-energy Particle Detector on board the CSES-01 Satellite. ApJ Lett., **945**, L39 (2023).

[15] Martucci M. et al. The First Ground-Level Enhancement of Solar Cycle 25 as Seen by the High-Energy Particle Detector (HEPD-01) on Board the CSES-01 Satellite. Space Weather, 21, 1 (2023)

[16] Modzelewska R. et al. Study of the 27 Day Variations in GCR Fluxes during 2007–2008 Based on PAMELA and ARINA Observations. The Astrophysical Journal, 904, 3 (2020)

[17] Ngobeni M. D. et. al. The 3D numerical modeling of the solar modulation of galactic protons and helium nuclei related to observations by PAMELA between 2006 and 2009, Astrophys. Space Sci. **365**, 182 (2020).

[18] Parker, E. N. Dynamical Theory of the Solar Wind. Space Science Reviews, 4, 666 (1965)

[19] Pesce-Rollins et al. Ion-rich acceleration during an eruptive flux rope event in a multiple null-point configuration Accepted for publication on ApJ (2025)

[20] Richardson, I.G. and Cane, H.V. Galactic Cosmic Ray Intensity Response to Interplanetary Coronal Mass Ejections/Magnetic Clouds in 1995–2009. Solar Physics, **270**, 609 (2011)

[21] Ruffolo D. et al. Monitoring short-term Cosmic rays spectral variations using Neutron Monitor time-delay Measurements, The American Astronomical Society, **817**, 1, 38, (2016)

[22] Tomassetti N. et al., Numerical modeling of cosmic-ray transport in the heliosphere and interpretation of the proton-to-helium ratio in Solar Cycle 24, Adv. Space Res. **64**, 2477 (2019)

[23] Banglieng, C. (2025). Cosmic-Ray Spectral Variations during 2007-2025 with Neutron Monitor Time-Delay Measurements at High Cutoff Rigidity. *PoS(ICRC2025)1273*.

[24] Bindi, V. (2025). HLEA and THIMON: Strengthening Neutron Monitor Observations from Haleakalā. *PoS(ICRC2025)1275*.

[25] Blanco Avalos, J. J. (2025). Solar event of May 11, 2024 some conclusions on the behavior of cosmic rays. *PoS(ICRC2025)1276*.

[26] Burom, S. (2025). Technical Design of the 1st Thai Space Consortium Satellite (TSC-1) and its Polar Orbiting Ion Spectrometer Experiment (POISE) Payload. *PoS(ICRC2025)1277*.

[27] Cervino Solana, P. (2025). Solar neutrons, an useful tool to study particle acceleration in the solar atmosphere. *PoS(ICRC2025)1278*.

[28] Cohen, C. (2025). The 23 July 2024 Fe-rich SEP event observed by Parker Solar Probe/Integrated Science Investigation of the Sun. *PoS(ICRC2025)1282*.

[29] Della Torre, S. (2025). COSMICA: A GPU-Optimized Code for Solar Modulation Studies. *PoS(ICRC2025)1285*.

[30] Fargion, D. (2025). Over-abundant gamma-like signals around Solar disk by smeared and bent electron pairs spiral. *PoS(ICRC2025)1291*.

[31] Hulsman, J. (2025). Comprehensive Study of the Lunar Energetic Particle Environment with LunPAN. *PoS(ICRC2025)1301*.

[32] Hyndman, R. (2025). Observations and simulations of decay phases of solar energetic particle events. *PoS(ICRC2025)1302*.

[33] Iuppa, R. (2025). Advancing Solar and Heliospheric Studies with the CSES Programme. *PoS(ICRC2025)1303*.

[34] Kawata, K. (2025). Observation of the Moon and Sun Shadows with the ALPAQUITA Air Shower Array in Bolivia. *PoS(ICRC2025)1308*.

[35] Kazmi, A. (2025). A Simulation Study of the Response of the Princess Sirindhorn Neutron Monitor (PSNM) and Bare Counters to Solar Neutrons. *PoS(ICRC2025)1309*.

[36] Koldobskiy, S. (2025). Are extreme solar particle events and superflares related? A probabilistic view. *PoS(ICRC2025)1311*.

[37] Kozai, M. (2025). Rigidity spectrum of cosmic-ray anisotropy observed by Global Muon Detector Network (GMDN). *PoS(ICRC2025)1315*.

[38] Laitinen, T. (2025). On the effect of turbulence on large-scale drifts of solar energetic particles. *PoS(ICRC2025)1318*.

[39] Leske, R. (2025). Observations of Solar Gamma-Ray Flares by ISIS/EPI-Hi/HET on Parker Solar Probe. *PoS(ICRC2025)1320*.

[40] Lui Y. (2025). Solar modulation of cosmic ray electron and positron flux up to 15 GeV measured with DAMPE. *PoS(ICRC2025)1325*.

[41] Luo, X. (2025). Study the relationship between Galactic Cosmic Rays' 27 day recurrent variation and Corotating Interaction Region. *PoS(ICRC2025)1326*.

[42] Luo, X. (2025). The numerical simulation of the Interplanetary Radiation Environment induced by Galactic Cosmic Rays. *PoS(ICRC2025)1327*.

[43] Matteucci, M. (2025). and 25th solar cycles: observations and results from the High-Energy Particle Detector (HEPD-01) onboard the CSES-01 satellite. *PoS(ICRC2025)1330*.

[44] Mazziotta, M. N. (2025). A 3D Monte Carlo calculation of the inverse Compton emission from the Sun and stars in presence of electromagnetic field. *PoS(ICRC2025)1331*.

[45] Menezes de Almeida, R (2025). Study of solar activity with AERA at the Pierre Auger Observatory. *PoS(ICRC2025)1332*.

[46] Mishev, A. (2025). Observation and analysis of the anisotropic Forbush decrease of 24 March 2024 *PoS(ICRC2025)1333*.

[47] Mishev, A. (2025). Spectra and anisotropy during GLE 74 on 11 May 2024 derived using neutron monitor data. *PoS(ICRC2025)1335*.

[48] Mitthumsiri, W. (2025). Hourly measurements of cosmic-ray spectral variation during Forbush decreases using ground-based neutron and muon detectors. *PoS(ICRC2025)1336*.

[49] Miyake, S. (2025). Cosmic-ray modulation over the past 10 years observed with CALET on the International Space Station. *PoS(ICRC2025)1337*.

[50] Ndiitwani, D. C. (2025). A modeling study of the solar modulation of galactic protons at lower energies over changing solar activity. *PoS(ICRC2025)1343*.

[51] Nuntiyakul, W. F. (2025). Response Functions of a Neutron Monitor from the 2023-24 Latitude Survey Aboard the Araon. Icebreaker*PoS(ICRC2025)1348*.

[52] Oshima, A. (2-25). Sola Neutron Events recorded by the Mt. Norikura Observatory during 2024. *PoS(ICRC25)1351*

[53] Palma, F. (2025). Multi-spacecraft observations of the 27-day periodicity in galactic protons from 2018 to 2019 by the HEPD-01 detector on board the CSES-01 satellite and other experiments. *PoS(ICRC2025)1352*.

[54] Perinelli, A. (2025). In-depth analysis of selected major solar events with the HEPP-L particle detector onboard CSES-01 in low-Earth orbit. *PoS(ICRC2025)1354*.

[55] Pesce-Rollins, M. (2025). Ion-rich acceleration during an eruptive flux rope event in a multiple null-point configuration. *PoS(ICRC2025)1355*.

[56] Puprasit, K. (2025). Design, Assessment, and Calibration of the Moon-Aiming Thai-Chinese Hodoscope for Observing Cosmic Ray Electrons, Solar Energetic Particles, and Lunar Albedo Ions. *PoS(ICRC2025)1357*.

[57] Raino', S. (2025). Surprising Variation of Gamma Rays from the Sun over the Solar Cycle Revealed with Fermi. *PoS(ICRC2025)1360*.

[58] Taricco, C. D. M. (2025). Scaler data from the Pierre Auger Observatory as a proxy of solar activity. *PoS(ICRC2025)1370*.

[59] Tomassetti, N. (2025). Modeling the heliospheric modulation of cosmic-ray in light of new data from AMS-02 in space. *PoS(ICRC2025)1371*.

[60] Usoskin, I. (2025). Cosmogenic ^{10}Be as a tracer of cosmic-ray variability: Atmospheric transport model and its parameterisation. *PoS(ICRC2025)1373*.

[61] Väisänen, P. (2025). Daily modulation parameter ϕ validated with AMS-02 for estimating GCR fluxes*PoS(ICRC2025)1374*.

[62] Väisänen, P. (2025). Hourly cadence cosmic ray modulation parameter ϕ at first glance: Challenges and possibilities. *PoS(ICRC2025)1375*.

[63] Wang, L. (2025). Solar Energetic Electron Events with a Spectral Bump Break. *PoS(ICRC2025)1378*.